Multicomponent Adsorption Equilibria of Nonideal Mixtures

Experimental gas-solid adsorption measurements were made on the binary and ternary mixtures of H_2S, CO_2, and C_3H_8 on H-mordenite molecular sieve zeolite at 30°C. The C_3H_8 containing binaries and the ternary mixture exhibited nonideal behavior, as evidenced by the azeotropelike crossovers in the composition domains and by the peaks in the total amount adsorbed surface. The ternary data were successfully predicted with the activity coefficients calculated by the spreading-pressure-dependent equation. Models that neglect the spreading-pressure dependence can only qualitatively predict the nonidealities.

Orhan Talu, Imre Zwiebel
Chemical and Bio Engineering Department
Arizona State University
Tempe, AZ 85287

Introduction

The prediction of multicomponent adsorption equilibria from single-component isotherm data has been only moderately successful, primarily because most models rely on the assumption that the adsorbate mixtures behave like ideal solutions. Myers and Prausnitz (1965) developed the adsorbate solution theory, which incorporates activity coefficients in the multicomponent isotherm equations to account for the deviations from ideality. These activity coefficients may be determined from experimentally measured multicomponent data or from theoretical correlations.

Noting the similarity between the liquid phase and the adsorbate phase, previous efforts (e.g., Costa et al., 1981) used well-known correlations derived for liquid systems to evaluate the adsorbate phase activity coefficients. While these equations may yield an acceptable match with experimental adsorption data for specific systems over a narrow range of conditions, they are inconsistent with thermodynamic criteria.

The liquid phase activity coefficients are functions of pressure, temperature, and composition, whereas the adsorbate phase activity coefficients are functions of spreading pressure, temperature, and composition (Myers and Prausnitz, 1965). The mixing models for liquid phases in equilibrium with vapors relate the activity coefficients to variations in composition, usually at constant temperature. These activity coefficient equations can be used to describe an adsorbate phase in equilibrium with a gas phase only if the spreading pressure is constant. Such an expression is inappropriate, because it is practically impossible to keep the spreading pressure constant during adsorption. For adsorption applications the gas phase pressure is usually specified, while the spreading pressure varies with composition even at constant gas pressure.

To overcome this deficiency the thermodynamically consistent spreading-pressure-dependent (SPD) equation was proposed (Talu, 1984) to evaluate adsorbate phase activity coefficients for nonideal systems. These activity coefficients could be used with the general adsorbate solution theory to predict or correlate multicomponent equilibria. The SPD equation utilizes the isosteric heats of adsorption obtained from single-component isotherms to incorporate the spreading-pressure dependency of the activity coefficients via lateral interaction potentials. While the SPD equation may be used in a predictive mode, whereby the adjustable parameters are evaluated from molecular properties, it is most effective when it is used in the correlative mode, using binary adsorption equilibrium data to provide highly reliable values for the parameters.

Since adsorbate systems that do not obey the ideal solution criteria received little attention in the past, the H_2S—CO_2—C_3H_8-mordenite system was chosen for study with the expectation that the adsorptive properties would exhibit nonideal behavior in the form of azeotropelike crossovers in the composition domain and maxima in the total amount adsorbed domain. The loci of the observed nonidealities, at constant pressure and temperature, are displayed on triangular equilibrium diagrams and the spreading pressure dependence of the activity coefficients has been verified. Special attention was paid to experimental design and the thermodynamic consistency of the data was demonstrated.

Adsorbate Solution Theory

In the adsorbate solution theory, the standard state is defined as the pure component adsorbate at the same spreading pressure and temperature as the mixture. Utilizing the equilibrium criteria of equal chemical potentials of each species in the gas and

adsorbate phases, Myers and Prausnitz (1965) derived the following equilibrium relation for gas adsorption:

$$Py_i = P_i^o x_i \gamma_i \quad \text{(constant T)} \tag{1}$$

where P_i^o is the gas phase pressure exerted by the adsorbate of single component i at the same spreading pressure and temperature as the mixture. Thus, P_i^o is the standard state gas pressure; it can be determined from the single-component adsorption isotherm. Equation 1, relating the intensive properties of adsorbate and gas phases, is similar to Rault's law for vapor-liquid equilibria, with vapor pressure replaced by P_i^o.

In order to fully describe a multicomponent adsorption system Eq. 1 must be accompanied by an expression describing the amounts adsorbed. One such relation for the total amount adsorbed is (Talu, 1984):

$$\frac{1}{n} = \sum \frac{x_i}{n_i^o} + \sum x_i \left(\frac{\partial \ln \gamma_i}{\partial \dfrac{\pi A}{RT}} \right)_{T,x} \quad \text{(constant T)} \tag{2}$$

where n_i^o is the amount of single-component i adsorbed at the standard state. Equation 2 can be obtained from the definition of molar area of mixing given by Myers and Prausnitz (1965) as:

$$a^m = a - \sum x_i a_i^o = RT \sum x_i \left(\frac{\partial \ln \gamma_i}{\partial \pi} \right)_{T,x} \quad \text{(constant T)} \tag{3}$$

Both Eqs. 2 and 3 illustrate that the adsorbate activity coefficients are functions of spreading pressure. This dependency can be eliminated only if the ideal solution assumption is invoked, or if the area of mixing is zero.

Adsorbate Phase Activity Coefficients

The assumption of ideal solution in the adsorbed phase (i.e., $\gamma_i = 1.0$) provides for simplified treatment of the adsorption data, which may be adequate for selected applications. Myers and Prausnitz (1965) showed that the idealization is quite satisfactory at low surface coverages and for systems where the active species have similar physical and adsorptive properties. In general, however, the ideal solution assumption may not be applicable for adsorption systems (Myers, 1983).

For nonideal systems it is necessary to develop a model in order to formulate an equation for the adsorbate phase activity coefficients. Three thermodynamic restrictions must be observed when adsorbate phase activity coefficients are defined:

1. Compliance with the definition of the standard state; i.e., the activity coefficient of a component in the mixture must approach unity as the composition of that component approaches unity:

$$\lim_{x_i \to 1.0} \gamma_i = 1.0 \tag{4}$$

2. At low surface coverages, as the spreading pressure approaches zero ideal solution behavior is approached and the activity coefficients of all components must approach unity:

$$\lim_{\pi \to 0} \gamma_i = 1.0 \tag{5}$$

This property of the adsorbate phase does not have an analog in bulk liquid phases. At pressures below the vapor pressure of the least volatile component the liquid phase ceases to exist. In adsorption, the adsorbate phase exists at all spreading pressures greater than zero, and the spreading pressure is zero only at zero gas pressure. The equations derived for the activity coefficients of liquid systems cannot meet this limitation; due to the absence of the spreading pressure functionality they can not anticipate the ideal behavior at low surface coverage.

3. Experimentally determined adsorbate phase activity coefficients must conform with the thermodynamic consistency test stipulated by the Gibbs-Duhem relation, which can be written for adsorbate mixtures (Talu, 1984) under isothermal conditions as:

$$\sum x_i \, d \ln \gamma_i = \left(\frac{1}{n} - \sum \frac{x_i}{n_i^o} \right) d \left(\frac{\pi A}{RT} \right) \quad \text{(constant T)} \tag{6}$$

The first term in parentheses is related to the area of mixing by:

$$\frac{a^m}{A} = \frac{1}{n} - \sum \frac{x_i}{n_i^o} \quad \text{(constant T)} \tag{7}$$

If a^m is zero the spreading-pressure dependency of the activity coefficient may be neglected. If the data were collected at constant spreading pressure and constant temperature, Eq. 6 would reduce to:

$$\sum x_i \, d \ln \gamma_i = 0.0 \quad \text{(constant T and } \pi\text{)} \tag{8}$$

It was pointed out by Myers (1983) that previous studies erroneously utilized Eq. 8 while performing the thermodynamic consistency check on isothermal and isobaric adsorption data.

The SPD Model

The superlattice model, similar to Gugenheim's (1952) quasi-chemical approach for liquid mixtures and its extension by Maurer and Prausnitz (1978), was adapted for the adsorbate phase and equations were developed that enable calculation of the adsorbate phase activity coefficients (Talu, 1984):

$$\ln \gamma_m = -s_m \ln \left(\sum_{j=1}^{C} \phi_j \alpha_{jm} \right) + s_m - s_m \sum_{j=1}^{C} \frac{\phi_j \alpha_{mj}}{\sum_{k=1}^{C} \phi_k \alpha_{kj}} \qquad \text{for } m = 1, \ldots, C \tag{9}$$

where s_m is the shape factor and

$$\phi_j = \frac{s_j \cdot x_j}{\sum_{i=1}^{C} s_i x_i} \tag{10}$$

with

$$\alpha_{ij} = \exp \left[-\tfrac{1}{2} z (e_{ij} - e_{jj}) / RT \right] \tag{11}$$

The single-component lateral interaction potentials e_{jj} can be determined from single-component isosteric heats of adsorption (Ross and Olivier, 1964):

$$e_{jj} = \frac{q_{j\pi}^{st} - q_{j0}^{st}}{\frac{1}{2}zMs_j} \tag{12}$$

where $q_{j\pi}^{st}$ is the isosteric heat of adsorption of single component j at the same spreading pressure as the mixture, and q_{j0}^{st} is the limiting isosteric heat of adsorption at zero coverage.

Similar to liquid mixtures (Abrams and Prausnitz, 1975), the cross-lateral interaction potentials e_{ij} can be stipulated as follows:

$$e_{ij} = \sqrt{e_{ii} \cdot e_{jj}}\,(1 - \beta_{ij}) \tag{13}$$

For spherical molecules of comparable size and adsorptive properties, statistical thermodynamic analyses indicate that $\beta_{ij} = 0.0$ (Abrams and Prausnitz).

Equations 9–13 can thus be used to evaluate the adsorbate phase activity coefficients. For a C-component mixture the procedure requires C shape factors s_i and $C(C-1)/2$ interaction correction parameters β_{ij}. The spreading-pressure dependency of the activity coefficients is incorporated by lateral interaction potentials, Eq. 12. The isosteric heats of adsorption for each species can be calculated as a function of spreading pressure from single component isotherms.

A purely predictive approach is possible if the interaction correction parameters β_{ij} are assumed to be equal to zero, and the shape factors can be calculated from molecular shapes and molecular dimensions of the constituent species. If it is further assumed that the molecules are lying flat in the hypothetical array of segments that constitute the adsorbate phase (Talu, 1984) a unique shape factor for each adsorbate species independent of the adsorbent properties can be found. However, since the adsorbate molecules are not always regularly oriented and may change orientation as adsorption proceeds (Ross and Olivier, 1964), this assumption may not yield satisfactory results.

Alternatively, the parameters can be determined from experimental single-component and binary adsorption equilibrium data (Talu, 1984). For a C-component mixture only $C + C(C-1)/2$ binary system experimental points are necessary to evaluate all the required parameters; however, there must be at least one point from every one of the binary combinations of the species present in the mixture.

The activity coefficients calculated using the SPD equation, Eq. 9, are illustrated in Figure 1 at constant gas pressure and in Figure 2 at constant gas composition for C_3H_8—CO_2 mixtures. In addition to the SPD equation data, the activity coefficients calculated by the predictive version of the SPD model and by the real adsorbate solution theory (RAST; Costa et al., 1981) are shown in these figures. The purely predictive model severely underestimates the nonidealities, although it does predict qualitatively the nonideal behavior. The RAST equation, which was derived for liquid systems and does not include spreading-pressure dependence of the activity coefficients, gives acceptable results in the constant gas pressure plane, Figure 1. This is not unexpected, since the spreading pressure does not vary greatly from the illustrated binary system. On the other hand, in the constant composition plane, as gas pressure (and spreading pressure) approaches zero the activity coefficients calculated with

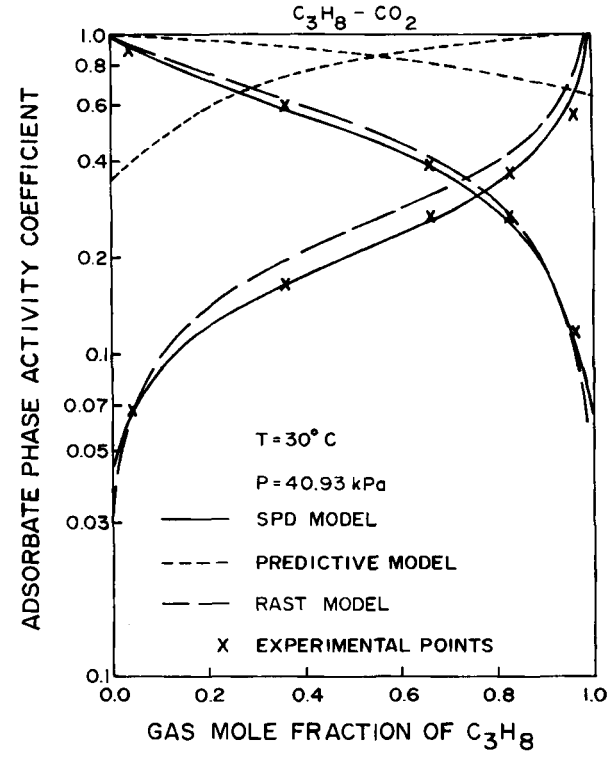

Figure 1. Adsorbate phase activity coefficients in constant pressure plane.
C_3H_8—CO_2—H-mordenite system

the RAST equation do not approach unity, Figure 2. This is in violation of the second thermodynamic criterion stated above.

In Figures 1 and 2 the experimental activity coefficients are also shown. These were evaluated by the equilibrium relationship, Eq. 1, from experimentally measured binary equilibrium data.

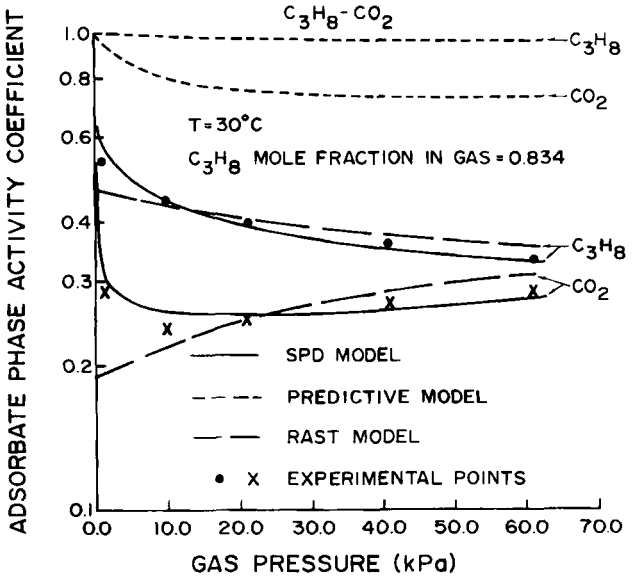

Figure 2. Adsorbate phase activity coefficients in constant composition plane.
C_3H_8—CO_2—H-mordenite system

Experimental

Hydrogen mordenite, in the form of 1/16 in (1.6 mm) pellets produced by Norton Company (Type Z-900H, Lot No. 75224), was activated in vacuum at 0.01 kPa and 320°C for 16 h. For consistent results the single-component and multicomponent experiments were conducted with adsorbent from the same production batch. Bone-dry carbon dioxide (99.8%) and hydrogen sulfide (99.5%) were purchased from Matheson Co.; instrument grade propane (99.5%) was purchased from Linde Co.

A block diagram of the experimental apparatus is shown in Figure 3; it is described in detail by Talu (1984). The gases from cylinders were further dried and cleaned by a series of beds packed with 5A molecular sieve and activated carbon. The flow of each component gas was separately controlled and metered. The gases were mixed and delivered to the adsorption section, which consisted of a fixed-bed adsorption chamber and a desorbate tank. The exit section contained an analyzer to monitor the effluent gas mixture for a qualitative indication of the exit composition, a back-pressure controller, the necessary scrubbers, and a vacuum source. Final equilibrium was stipulated when the inlet and outlet gas streams to the adsorber had equal compositions for at least 1 h as measured with a gas chromatograph.

Both adsorbed material and gas phase contents of the adsorption chamber were transferred to the previously evacuated, known-volume desorbate tank by heating the adsorbent to 320°C and cooling the desorbate tank with liquid nitrogen. After desorption was complete and the desorbate tank temperature returned to ambient, the desorbate tank pressure was recorded and the gas was sampled for analysis.

The amount adsorbed of each component was determined by subtracting the amount of equilibrium gas in the void space of the adsorption chamber from the desorbate tank contents. The amount of gas in the interstitial gas space was calculated by ideal gas law with the previously measured void volume.

All pressure measurements were taken with a MKS Baratron differential pressure gage with a vacuum manometer on the reference side. The accuracy of pressure measurements was ±0.005 kPa, limited by the accuracy of the cathetometer. Temperature measurements had an accuracy of ±0.1°C, and the accuracy of composition was ±0.1 mol %, assured by repeated samples of the gas. Thus the precision of amounts adsorbed data was estimated to be ±0.05 mmol/g, or an average of about ±5%.

Experimental design (ternary system)

Particularly in the case of ternary systems, the complexity and time requirements of the experiments dictated a careful experimental design whereby a minimum number of experiments would provide the necessary confirmation of the hypotheses with a maximum degree of confidence. According to the modified phase rule for adsorption systems (Ross and Olivier, 1964; Myers and Prausnitz, 1965) a three-component adsorbate system has four degrees of freedom. Therefore, even at constant temperature a four-dimensional domain would be necessary to present the three independent variables (pressure and two gas phase compositions) along with a dependent variable (amount adsorbed or adsorbate composition). To describe the experimental design Figure 4 presents an orthogonal representation of the pressure-composition domain at constant temperature (30°C), with the compositions of all three components being presented in the conventional equilateral triangular diagram. In Figure 4 the location of the experimental points is given. A series of experiments was run at various gas pressures with a fixed gas composition of equal concentration to the three components ($y_i \sim 0.33$) along the path AB. In addition, experiments were run at P = 13.35 kPa, illustrated in the constant pressure plane CEG. These constant pressure experiments can be organized in two different ways:

1. Constant gas composition paths, i.e., path QR (constant y_{CO_2}), path MN (constant y_{H_2S}), and path KL (constant $y_{C_3H_8}$)
2. Constant gas composition ratios, i.e. path GH ($y_{H_2S}/y_{C_3H_8}$ = constant), path EF (y_{H_2S}/y_{CO_2} = constant), and path CD ($y_{C_3H_8}/y_{CO_2}$ = constant).

Straight lines drawn through the points along a constant gas composition path terminate in binary mixture points at the sides of the triangular domain (points K, L, M, N, Q, and R). Straight lines connecting the points along a constant gas composition ratio path, on the other hand, can be extrapolated to one of the vertices (C, E, and G) that represent a pure single-component system. The latter organization is preferred because it provides an expeditious and convenient route to the evaluation of the spreading pressures.

Experimental spreading pressures

In applying the Myers and Prausnitz (1965) equilibrium equation, the standard state pressure, P_i^o, has to be evaluated from single-component data at the same spreading pressure and temperature as the equilibrium mixture. Thus, to evaluate the spreading pressures at any point in the multicomponent adsorption space, the Gibbs adsorption equation

$$d\left(\frac{\pi A}{RT}\right) = n(J)\, d\ln P + \sum n(J) x_i\, d\ln y_i \qquad (14)$$

has to be integrated at constant temperature from $P = 0$, where $\pi = 0$, to the experimental pressure and composition of the point

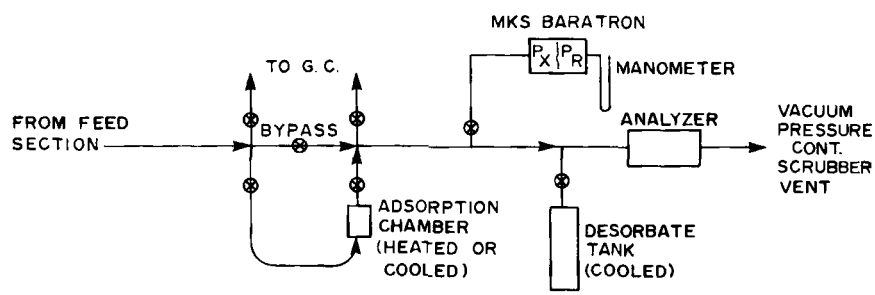

Figure 3. Diagram of experimental apparatus.

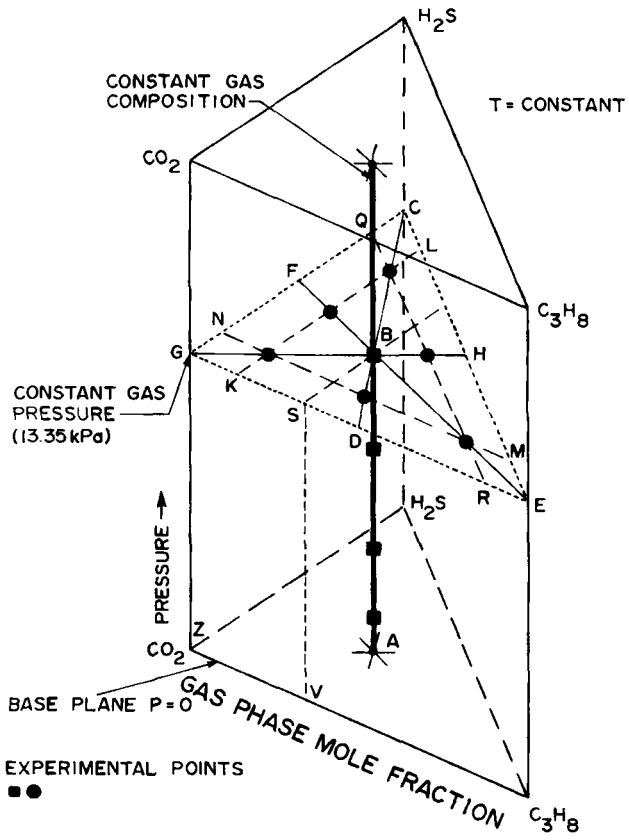

Figure 4. Orthogonal representation of adsorption space for ternary mixture at T = 30°C.

in question. Since spreading pressure is a point function, several different integration paths can be identified along the pertinent domain. For example, the spreading pressures of binary mixtures could be evaluated along two main paths:

1. Integration along a constant gas composition within the binary domain from $P = 0$ (where $\pi = 0$) to the pressure of the mixture

$$\pi_B = \int_o^P n(2)\, d \ln P \tag{15}$$

2. Integration in a one-component plane from $P = 0$ (where $\pi = 0$) to the pressure of the mixture followed by integration in the constant pressure plane to the mixture composition

$$\pi_B = \int_o^P n(1)\, d \ln P + \int_{0,0}^{y_1} n(2)\left(\frac{x_1}{y_1} - \frac{x_2}{y_2}\right) dy_1 \tag{16}$$

This second alternative could be accomplished from opposite directions, depending on which component is chosen for the first integration. Table 1 illustrates these results for one point in each of the three binary mixtures, and it shows that the values of the spreading pressure obtained along the various paths are within 5% of each other.

For the three-component system, the alternatives to evaluate the spreading pressure at point B are illustrated in Figure 4. Four different basic types of paths can be identified:

Path AB (constant composition, variable pressure in ternary domain):

$$\left(\frac{\pi A}{RT}\right)_B = \int_0^P n(3)\, d \ln P \tag{17}$$

Path VSB (constant composition variable pressure in binary domain followed by constant pressure variable composition in ternary domain):

$$\left(\frac{\pi A}{RT}\right)_B = \int_0^P n(2)\, d \ln P + \int_S^B n(3)\left(\frac{x_{H_2S}}{y_{H_2S}} - \frac{x_{CO_2}}{y_{CO_2}}\right)_{SB} dy_{H_2S} \tag{18}$$

Path $ZGSB$ (single-component variable pressure, followed by constant pressure variable composition in binary domain, followed by constant pressure variable composition in ternary domain):

$$\left(\frac{\pi A}{RT}\right)_B = \int_0^P n(1)\, d \ln P + \int_G^S n(2)\left(\frac{x_{CO_2}}{y_{CO_2}} - \frac{x_{C_3H_8}}{y_{C_3H_8}}\right)_{GS} dy_{CO_2} + \int_S^B n(3)\left(\frac{x_{H_2S}}{y_{H_2S}} - \frac{x_{CO_2}}{y_{CO_2}}\right)_{SB} dy_{H_2S} \tag{19}$$

Path ZGB (single-component variable pressure followed by constant pressure variable composition in ternary domain):

$$\left(\frac{\pi A}{RT}\right)_B = \int_0^P n(1)\, d \ln P - \int_G^B n(3) \cdot \left[\frac{1}{1+r} \cdot \frac{x_{H_2S}}{y_{H_2S}} + \frac{r}{1+r} \cdot \frac{x_{C_3H_8}}{y_{C_3H_8}} - \frac{x_{CO_2}}{y_{CO_2}}\right]_{GB} dy_{CO_2} \tag{20}$$

where $r = y_{C_3H_8}/y_{H_2S}$, the constant ratio of the gas phase compositions along the path GH.

In Eqs. 18–20 the limits of integration are the mole fractions of the designated component (in the differential term) at the point specified by the appropriate letter symbol in Figure 4. Also, a special notation was used in Eq. 14–20 designating the variable n with a parenthetic number (J), so that $n(J)$ repre-

Table 1. Binary Mixture Spreading Pressures

Eq. No.	Integration Along: Pressure Path	Integration Along: Composition Path	Spreading Pressure*
	CO_2—H_2S binary; y_{CO_2} = 0.812, P = 15.55 kPa		
15	4.76 (mix)	—	4.76
16	7.08 (H_2S)	−2.30	4.78
16	2.87 (CO_2)	1.90	4.77
	C_3H_8—CO_2 binary; $y_{C_3H_8}$ = 0.833, P = 41.03 kPa		
15	4.98 (mix)	—	4.98
16	4.22 (CO_2)	0.70	4.92
16	3.51 (C_3H_8)	1.46	4.97
	C_3H_8—H_2S binary; $y_{C_3H_8}$ = 0.960, P = 8.11 kPa		
15	3.34 (mix)	—	3.34
16	5.82 (H_2S)	−2.52	3.30
16	2.11 (C_3H_8)	1.21	3.32

*Valves in mmoles/gm; T = 30°C

sents the total amount adsorbed of a J-component mixture. Finally, to properly describe the constant composition ratio paths in the constant pressure plane:

- Path CD was designated as the H_2S path, where $y_{CO_2}/y_{C_3H_8}$ = constant
- Path EF was designated as the C_3H_8 path, where y_{H_2S}/y_{CO_2} = constant
- Path GH was designated as the CO_2 path, where $y_{H_2S}/y_{C_3H_8}$ = constant

since the composition of the specified species varies from $y_i = 0$ to $y_i = 1.0$ along the designated path.

Thus, to evaluate the spreading pressure at point B it is necessary to have data with different degrees of complexity, depending on the paths used for the integration. In Table 2 the requirements for some of these calculations are summarized, corresponding to the paths indicated above. Of course, integration along other combinations of paths could be used to evaluate the spreading pressure at point B, provided that the lower limit of the integrals is known. While thermodynamically the value of the spreading pressure is uniquely defined at a given point by the prevailing temperature, pressure, and composition, in practice its accuracy is a function of the integration path, as illustrated in Table 2.

The ternary experimental results described in this paper were organized primarily according to the fourth mode described above, i.e., Eq. 20, so that single-component integration along the pressure axes followed by ternary mixture integrations along the constant composition ratio paths enabled expedient correlation of the data. The experimental points were carefully selected so that the data could also be organized in a secondary direction, along the constant composition paths.

Results

The single-component adsorption isotherms of hydrogen sulfide, carbon dioxide, and propane on the hydrogen mordenite were experimentally determined, Table 4. The affinity of the adsorbent for each of these gases can be related to their electronic properties since their critical diameters are small enough to allow free entry even to side cavities of the hydrogen mordenite, Table 3. As expected, the order of preferential adsorption was found to be $H_2S > CO_2 > C_3H_8$, although at low surface coverages, 0.2–0.6 mmole/g, propane was adsorbed slightly more than carbon dioxide.

Table 2. Integration Paths for Evaluation of Ternary Mixture Spreading Pressures

Total Path	Eq. No.	Variable Pressure Integration Path	J	π_P	Integration in Constant Pressure Plane Path	J	Constraint	π_C	π_B
AB	17	AB	3	5.922	—	—	—	—	5.92
VSB	18	VS	2	4.755	SB	3	$y_{C_3H_8}$ = constant	1.150	5.90
ZGSB	19	ZG	1	2.717	GS	2	$y_{H_2S} = 0$	1.945	5.81
					SB	3	$y_{C_3H_8}$ = constant	1.150	
ZGB	20	ZG	1	2.717	GB	3	$\frac{y_{C_3H_8}}{y_{H_2S}}$ = constant	3.160	5.81

π_B = spreading pressure at point B, mmole/g
π_c = spreading pressure evaluated in constant-pressure plane, mmol/g
π_P = spreading pressure evaluated along variable pressure path, mmol/g
J = number of components in mixture used for integration

Table 3. Molecular Properties of Experimental Species

Property	Source*	CO_2	H_2S	C_3H_8
Molecular dia., Å	1	3.23	3.24	4.05
Dipole moment, μDebye	2	0.00	0.92	0.00
Avg. polarizability, $cm^3 \times 10^{24}$	3	2.65	3.78	6.29
Quadrupole moment, $esu/cm^2 \times 10^{26}$	4	3.12	—	—

*1. Ross and Olivier (1964)
2. Moore (1962)
3. Barrer (1966)
4. Kingston and Macleod (1959)

Isosteric heats of adsorption were evaluated by the standard procedure of crossplotting the logarithm of pressure vs. the inverse absolute temperature at constant amount adsorbed (Ross and Olivier, 1964). The slopes of the straight-line isosteres were measured, and were used in the activity coefficient calculations by the SPD equation.

Binary mixture isotherms

Graphical representation of a binary adsorption isotherm requires a three-dimensional coordinate system with total gas pressure, gas composition, and amount adsorbed as the axes. However, for experimental convenience and ease of visualization the data are presented in two-dimensional cross section subdomains; either in a constant-pressure plane or in a constant-composition plane. Equilibrium capacity measurements taken at 30°C for the three binary mixtures, CO_2—H_2S, C_3H_8—CO_2, C_3H_8—H_2S, are shown in Figure 5 at constant gas pressure. Note that direct comparisons cannot be made on these graphs because the gas pressures are different for the three binary mixtures. The data are also given in Table 5.

The experimental results show that the degree of nonideality of the binary mixtures, as defined by the values of the activity coefficients, increases in the order of CO_2—H_2S < C_3H_8—CO_2< C_3H_8—H_2S. The CO_2—H_2S mixture would be expected to exhibit strongly nonideal behavior because of the interactions of highly polar molecules; this mixture is known to exhibit nonidealities in the liquid phase. However, as suggested by some investigators (Perfetti and Wightman, 1976), the strong adsorbent-adsorbate interactions can outweight the adsorbate-adsorbate interactions, so that the equilibrium data do not show any visible evidence of nonideality, Figure 6.

In the constant gas pressure plane, Figure 5, the C_3H_8—CO_2 and C_3H_8—H_2S mixtures exhibit nonideal behavior indicated by the peaks in the total amount adsorbed vs. gas composition plots. Also, these mixtures have azeotropelike crossovers on the x-y diagrams, as shown in Figures 7 and 8. According to some authors the azeotropic behavior would be expected for the C_3H_8—CO_2 binary mixture, because the pure-component isotherms intersect (Hyun and Danner, 1982). However, no such intersection was found for the C_3H_8—H_2S system. Therefore, the rule of thumb method is not sufficient to predict the existence of nonidealities.

The observation of the nonidealities may be explained qualitatively by the electronic and size characteristics of the species, Table 3. Hydrogen sulfide is a small polar molecule held very strongly by the ionic sites of the hydrogen mordenite. The CO_2

Table 4. Single-Component Equilibrium Data on H-mordenite

(P in kPa, n in mmoles/gm)

P	n	P	n	P	n	P	n	P	n
					Carbon Dioxide				
T = 10.0 C		43.67	2.16	5.08	0.78	50.46	1.81	1.14	0.26	62.06	1.45
		50.12	2.24	6.02	0.84	53.63	1.83	1.71	0.31	69.91	1.52
0.32	0.38	60.76	2.36	6.88	0.86	60.84	1.90	2.17	0.34	78.40	1.59
0.47	0.45			7.51	0.92	68.94	1.97	2.25	0.34	87.41	1.65
0.75	0.53	T = 30.0 C		8.22	0.92	76.62	2.04	3.53	0.42	96.00	1.70
1.12	0.63			9.59	1.01	85.06	2.10	4.46	0.47	108.74	1.78
1.91	0.77	0.37	0.25	11.74	1.07	93.19	2.15	4.99	0.49	122.19	1.84
3.03	0.92	0.57	0.29	12.71	1.13	101.19	2.20	6.74	0.56	133.44	1.90
4.48	1.04	0.63	0.31	14.67	1.20	110.63	2.25	8.80	0.64	143.73	1.96
6.85	1.21	0.72	0.32	17.71	1.28	119.18	2.29	11.78	0.73	159.03	2.03
10.97	1.43	0.94	0.36	19.87	1.30	126.52	2.33	16.48	0.84	180.13	2.11
13.68	1.53	1.20	0.40	23.20	1.39	135.71	2.37	22.06	0.96	214.47	2.21
18.85	1.70	1.57	0.45	27.50	1.49	138.67	2.38	27.92	1.06	228.05	2.25
22.72	1.80	2.97	0.60	28.29	1.49			34.07	1.15	254.73	2.33
26.59	1.88	3.63	0.68	34.13	1.58	T = 50.0 C		40.20	1.22	271.62	2.38
31.48	1.98	4.24	0.73	40.29	1.67			46.91	1.30	292.86	2.44
37.43	2.07	4.56	0.73	46.72	1.75	0.63	0.21	54.37	1.38		
					Hydrogen Sulfide				
T = 10.0 C		4.83	1.98	1.70	1.30	25.95	2.26	5.92	1.21	T = 95.0 C	
		5.87	2.06	1.89	1.38	27.62	2.28	7.83	1.30		
0.41	1.13	7.09	2.13	2.57	1.45			11.02	1.42	3.19	0.64
0.54	1.21	8.61	2.21	3.32	1.51	T = 65.0 C		14.82	1.51	5.27	0.83
0.66	1.28	9.83	2.27	4.03	1.57			17.94	1.59	17.81	1.22
0.84	1.35			4.87	1.63	0.48	0.39	22.44	1.67	33.56	1.45
0.94	1.42	T = 30.0 C		5.73	1.69	0.55	0.48	25.66	1.72	54.32	1.66
1.10	1.48			6.78	1.75	0.68	0.51	31.70	1.81	77.47	1.81
1.30	1.54	0.49	0.89	8.09	1.82	0.85	0.60	38.63	1.91	101.87	1.95
1.52	1.59	0.58	0.96	9.60	1.88	1.16	0.72	46.49	1.98		
1.87	1.65	0.76	1.03	11.67	1.96	1.62	0.81	54.16	2.05		
2.28	1.72	0.86	1.10	14.32	2.04	2.21	0.90	62.07	2.11		
2.67	1.78	1.10	1.16	17.10	2.11	2.62	0.97	70.31	2.17		
3.07	1.84	1.36	1.23	20.26	2.18	4.11	1.10	79.18	2.24		
					Propane				
T = 9.9 C		5.35	0.82	T = 30.0 C		4.72	0.69	193.37	1.22	16.88	0.74
		7.03	0.86			5.06	0.70	206.81	1.24	22.01	0.77
0.02	0.10	9.26	0.89	0.10	0.09	7.39	0.75			28.53	0.81
0.04	0.14	11.00	0.92	0.14	0.12	10.26	0.79	T = 51.1 C		36.22	0.84
0.05	0.19	15.32	0.96	0.22	0.18	12.67	0.81			45.16	0.86
0.09	0.24	20.23	1.00	0.33	0.24	16.70	0.85	0.51	0.17	55.76	0.89
0.12	0.29	24.92	1.04	0.41	0.30	24.81	0.90	0.67	0.22	67.18	0.92
0.16	0.34	30.49	1.07	0.49	0.31	34.28	0.95	0.91	0.28	78.27	0.94
0.22	0.39	37.07	1.09	0.57	0.36	43.85	0.98	1.21	0.33	90.35	0.96
0.30	0.44	42.61	1.11	0.77	0.41	54.62	1.02	1.80	0.40	111.84	0.99
0.43	0.49	49.18	1.13	0.99	0.44	65.79	1.04	2.63	0.46	126.53	1.01
0.62	0.55	59.65	1.16	1.08	0.48	73.19	1.06	4.02	0.53	141.79	1.03
0.95	0.61	71.26	1.19	1.47	0.51	94.66	1.09	5.43	0.58	159.59	1.05
1.44	0.66	93.21	1.23	1.51	0.53	115.89	1.14	6.92	0.61	178.21	1.07
2.11	0.71	114.96	1.26	2.27	0.59	140.07	1.17	8.81	0.64	199.44	1.10
2.97	0.75			2.40	0.59	158.90	1.19	11.12	0.69	207.51	1.10
4.04	0.78			3.22	0.64	174.76	1.20	13.69	0.71		

P in kPa; n in mmol/g.

molecule, comparable in size to the H_2S molecule, is polarizable and it has a quadrupole. Propane is about twice the size of other species and it is only mildly polarizable. Since all molecules are small enough to enter the pore structure, competitive adsorption prevails in all these mixtures. In the CO_2—H_2S binary system both species compete for the same sites since they are comparable in size and both are electronically active. The result is an isotherm that is essentially proportional to the relative amounts of the species, with the hydrogen sulfide dominating in the adsorbate phase because of its higher charge distribution. On the other hand, in the propane-containing mixtures there are different interactions at low-propane and high-propane compositions. When propane molecules are present in relatively small concentrations, they can be positioned at random locations in the pore space, not being specifically attracted to the ionic adsorption sites. Thus the propane adsorption has little hindrance from the adsorption of the highly site-specific CO_2 or H_2S. This lack of competition results in an increased total amount adsorbed and in exaggerated propane compositions in the adsorbate phase. As the propane content of the mixture is increased, there is greater competition between molecules of two different species because of the space limitations. The smaller

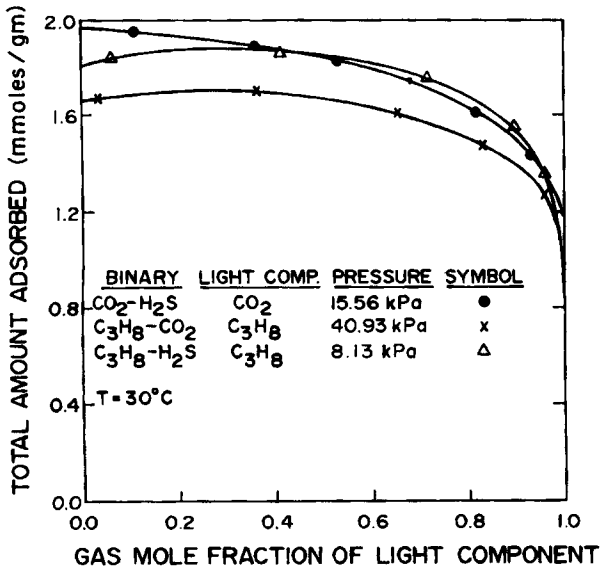

Figure 5. Binary adsorption equilibrium curves in constant pressure plants.
Total amounts adsorbed vs. gas composition

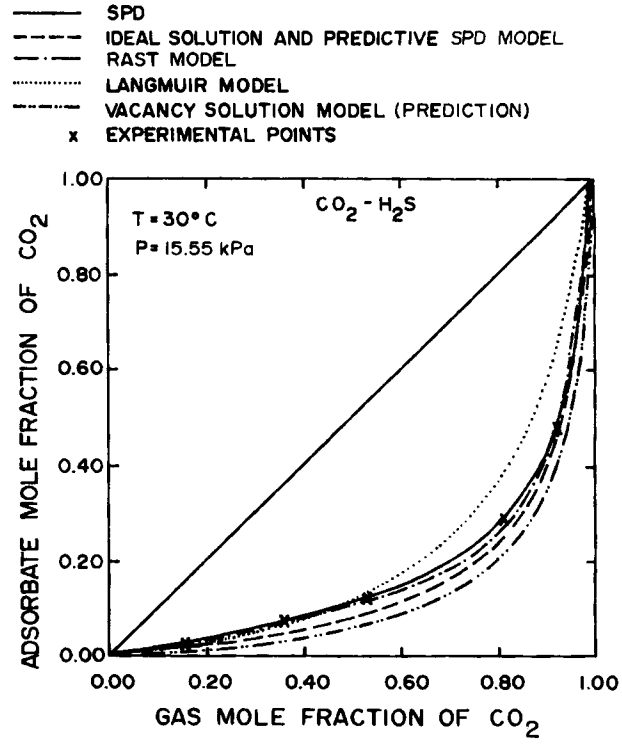

Figure 6. Equilibrium composition diagram.
CO_2—H_2S—H-mordenite system

CO_2 or H_2S molecules (being site-specific they are strongly held) will not be affected by the space limitations, while there will be a limit to the number of the larger C_3H_8 molecules that will fit into the pores. Thus propane adsorption is suppressed relative to its increased concentration in the gas phase, and this results in a reversal in the relative affinity of the adsorbent for the propane. Hence the development of an azeotropelike crossover.

Thermodynamic Consistency

Both the experimental activity coefficients and those calculated by the SPD equation obey the first two of the thermodynamic limitations described above, Figures 1 and 2. The activity coefficients also conform with the thermodynamic consistency check, as shown for a typical example of C_3H_8—H_2S data in Table 6. The consistency check was performed by the application of the integral form of Gibbs-Duhem equation given in Eq. 6. In Table 6 the values of integrals on the lefthand side of the equation are given in columns *2* and *3*, while the value of the integral on the righthand side is given in column *5*; each integral was evaluated over the composition range given in column *1*. The integrand on the righthand side is related to the area of mixing (a^m/A), and its average value over each corresponding concentration range is given in column *4*. These data are presented to demonstrate Myers' (1983) contention that neglecting the righthand side of Eq. 6 when making a consistency check can result in significant errors. This assumption would be acceptable if either the spreading pressure were constant or the area of mixing were zero. However, the spreading pressure can not be kept constant *a priori*, and the values in Table 6 column *4* show that the area of mixing is numerically significant as compared to the other terms of Eq. 6. Thus, by using the entire Gibbs-Duhem equation the consistency of the data is demonstrated by the

Table 5. Binary Adsorption Data of CO_2, H_2S, and C_3H_8 Mixtures on H-mordenite at 30°C

CO_2—H_2S				C_3H_8—CO_2				C_3H_8—H_2S			
P kPa	y_{CO_2}	n mmol/g	x_{CO_2}	P kPa	$y_{C_3H_8}$	n mmol/gm	$x_{C_3H_8}$	P kPa	$y_{C_3H_8}$	n mmol/gm	$x_{C_3H_8}$
					Constant Composition Plane						
0.60	0.771	0.738	0.187	1.29	0.833	0.662	0.712	1.85	0.959	0.960	0.525
0.62	0.784	0.645	0.188	10.11	0.835	1.093	0.651	4.87	0.969	1.181	0.515
7.00	0.788	1.378	0.211	21.41	0.837	1.287	0.626	8.11	0.960	1.357	0.476
12.17	0.795	1.548	0.217	41.03	0.833	1.475	0.594	18.32	0.965	1.580	0.463
—	—	—	—	61.19	0.822	1.595	0.566	—	—	—	—
					Constant Pressure Plane						
15.55	0.819	1.614	0.265	—	—	—	—	8.13	0.064	1.851	0.084
14.38	0.160	1.945	0.032	40.88	0.042	1.670	0.199	8.14	0.416	1.863	0.218
14.93	0.362	1.886	0.078	41.55	0.367	1.705	0.423	8.30	0.721	1.762	0.299
15.69	0.536	1.826	0.128	40.95	0.662	1.611	0.510	7.97	0.897	1.558	0.400
15.77	0.934	1.436	0.462	40.86	0.965	1.271	0.727				

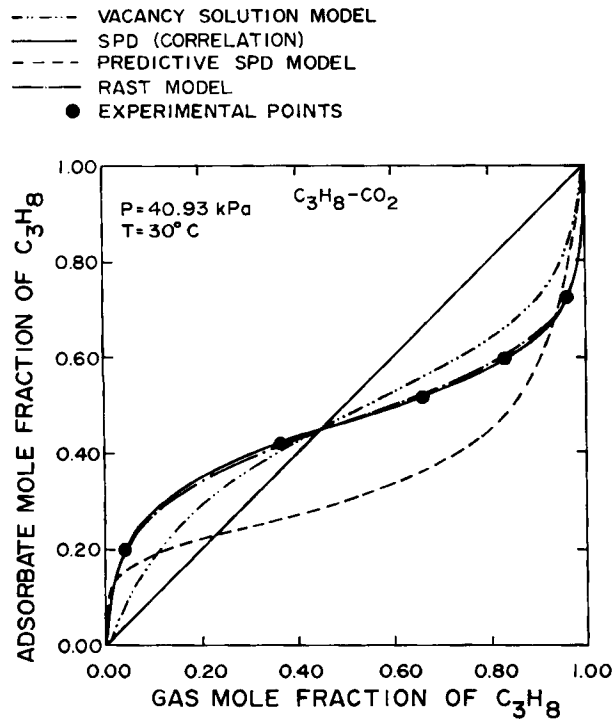

Figure 7. Equilibrium composition diagram.
C_3H_8—CO_2—H-mordenite system

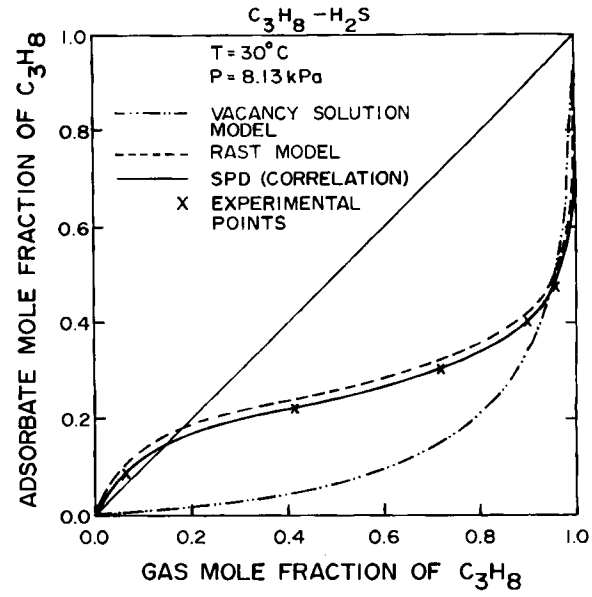

Figure 8. Equilibrium composition diagram.
C_3H_8—H_2S—H-mordenite system

small values in column 6, no greater than 3% of the corresponding terms evaluated from the equation.

Binary Isotherm Predictions/Correlations

Since the CO_2—H_2S data do not visibly exhibit nonideal characteristics, they were compared with predictions with the ideal solution model (Myers and Prausnitz, 1965), the mixed Langmuir model (Markam and Benton, 1931), and more general models such as the RAST Model (Costa et al., 1981), the vacancy solution model (Suwanayuen and Danner, 1980), and the predictive mode of the SPD equation (Talu, 1984). None of these models was very successful in predicting the data; see Figure 6. This is not surprising since there is some degree of nonideality in the data as shown by the activity coefficients.

The propane-containing binary systems exhibited the nonidealities by azeotropelike crossovers in the composition curves, Figures 7 and 8, and they would not be expected to conform to any of the ideal models. The SPD equation in the predictive mode predicted the existence of a crossover, but did not predict the composition data with acceptable accuracy. The vacancy solution model predicted the location of the crossover in the C_3H_8—CO_2 data but it was only moderately successful in predicting the balance of the compositions. The vacancy solution model failed with the C_3H_8—H_2S system; it did not even predict the crossover. This is believed to be due to the precision of the single-component parameters, particularly those corresponding to the monolayer coverage, and Henry's law constants for the H_2S are not adequate to provide the successful predictions.

The RAST and the SPD models, utilizing the binary data to evaluate the necessary parameters, did an excellent job of correlating the data of the entire composition region for all three binary systems.

Ternary mixture isotherms

The experimental three-component results are presented in Figure 9 along the constant composition but variable pressure path *AB*, Figure 4, and in Figures 10–14 along a constant pressure plane *CEG*. All these data are tabulated in Table 7.

Table 6. Thermodynamic Consistency of C_3H_8—H_2S Binary Data on Hydrogen Mordenite

H_2S Adsorbate Composition Range (1)	Integrals on LHS $\int x_{C_3H_8} d\ln\gamma_{C_3H_8}$ (2)	Integrals on LHS $\int x_{H_2S} d\ln\gamma_{H_2S}$ (3)	Avg. Value of Integrand on RHS a^m/Å (4)	Integral on RHS (5)	Difference, RHS − LHS (6) = (5)−(3)−(2)
1.000–0.916	−0.07500	0.07557	0.00778	0.00143	0.00200
0.916–0.782	−0.15466	0.16589	0.03850	0.00920	0.00203
0.782–0.701	−0.15230	0.20902	−0.08060	0.05637	0.00035
0.701–0.601	−0.15267	0.27788	−0.12336	0.12571	−0.00050
0.601–0.524	−0.15911	0.26891	−0.15483	0.10945	0.00035
0.524–0.000	−0.44301	0.54537	−0.08152	0.10036	0.00200

Integrated form of Eq. 6.
Pressure, 8.13 kPa; temperature, 30°C.
LHS = lefthand side of equation.
RHS = righthand side of equation.

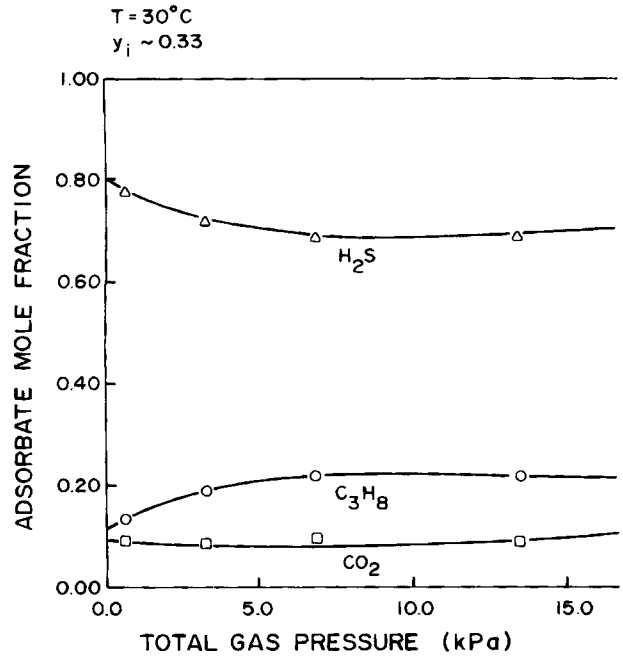

Figure 9. Adsorbate phase compositions as a function of pressure for ternary mixture.

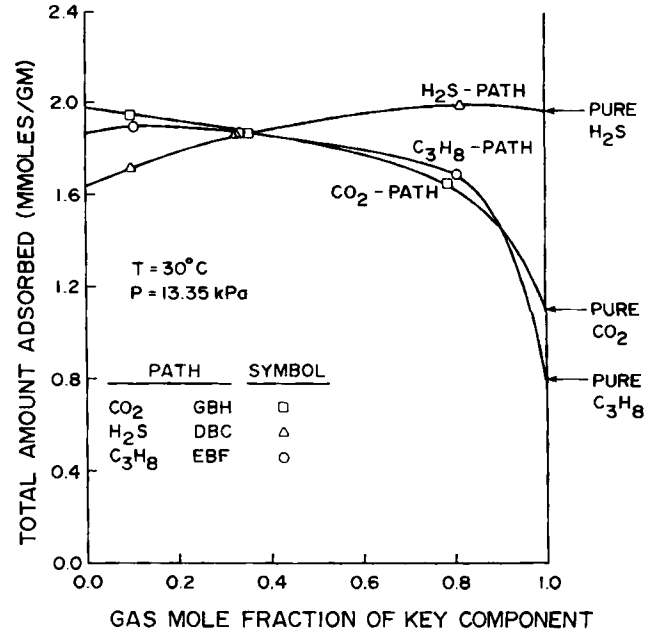

Figure 10. Ternary adsorption isotherms in constant pressure plane.
Total amount adsorbed along the three constant composition ratio paths.

As the pressure increases the partial amounts adsorbed of each of the three components increases; however, at any given pressure the amount adsorbed of each component is significantly lower than its corresponding single-component loading. The selectivity for the components remains essentially constant as the pressure is increased above $P > 3$ kPa, Figure 9.

The constant pressure data are presented, as outlined above, along the three component paths (i.e., at constant gas composition ratios). The total amount adsorbed curves have maxima along the H_2S path (CD) and along the C_3H_8 path (EF), Figure 10, indicating an adsorption capacity peak in the trisection of the composition space nearest to the H_2S vertex.

Figures 11, 12, and 13 show the variations in composition along the three composition paths. In each of these figures all three adsorbed phase compositions are plotted along the ordinate vs. the gas phase composition of the designated component along the abscissa. Also, in each of these figures there are two straight lines corresponding to $x_i = y_i$, along which the adsorbed phase compositions of the identified component equal the gas phase compositions. Wherever the appropriate component curve crosses its corresponding equal-composition line, an azeotropelike composition crossover exists, indicating a nonideality in the system. Several such crossover points were found in the P = 13.35 kPa constant pressure plane:

- Along the H_2S path (CD) in Figure 11 a C_3H_8 crossover (point a)
- Along the H_2S path (CD) in Figure 11 an H_2S crossover (point b)
- Along the CO_2 path (GH) in Figure 12 a C_3H_8 crossover (point c)
- Along the C_3H_8 path (EF) in Figure 13 a C_3H_8 crossover (point d)
- Along the C_3H_8 path (EF) in Figure 13 a CO_2 crossover (point e)

Additional crossover points (f, g, and h) were located along the constant composition paths (Talu, 1984). On the triangular constant pressure plane, Figure 14, these points can be connected to give the loci of all crossover points in the composition domain. These loci, as expected, intersect the edges of the triangle, which represent the two component mixtures, at the actual location of the binary composition crossovers (Talu 1984). The composition domain is thus divided into four regions (labeled with roman numerals) and in each region the appropriate inequality identifies the prevailing relationship between the adsorbed phase composition and the gas phase composition of each component (that is, whether the points are above or below the equal-composition lines). Regions I and II are separated by the locus of C_3H_8 crossovers, regions I and III are separated by the locus of H_2S crossovers, and regions II and IV are separated by the locus of CO_2 crossovers.

These azeotropelike phenomena are related to the change in the propane adsorption mechanism. At low C_3H_8 compositions, regions I and III, the strongly adsorbed H_2S and/or CO_2 molecules are preferentially attached to the active sites, leaving the pore space available for adsorption of C_3H_8 molecules in excess of the gas phase composition. As the propane composition is increased, regions II and IV, size considerations limit the number of the larger C_3H_8 molecules that can enter the pores, while the site-specificity still controls the adsorption of the H_2S and/or CO_2. Therefore, a reversal in the C_3H_8 composition in the adsorbed phase occurs at the boundary $\overline{LhadcfD}$, which is the locus of the C_3H_8 crossovers.

Similarly, the loci of the CO_2 and H_2S crossovers are related to the competition between species. As the two-component compositions along the edges of the triangle are extended to three-component mixtures within the triangle, the azeotropelike behavior of the species is also translated into the ternary domain.

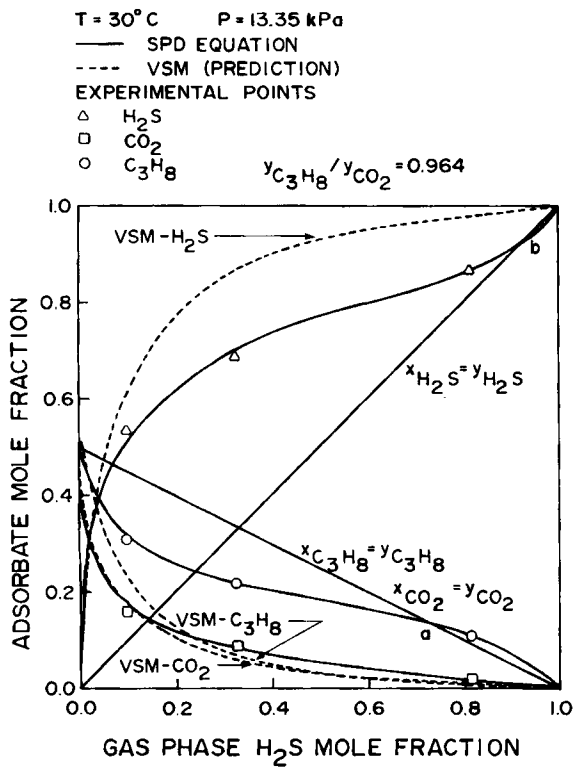

Figure 11. Ternary adsorbed phase compositions along H_2S path (path *CD*).

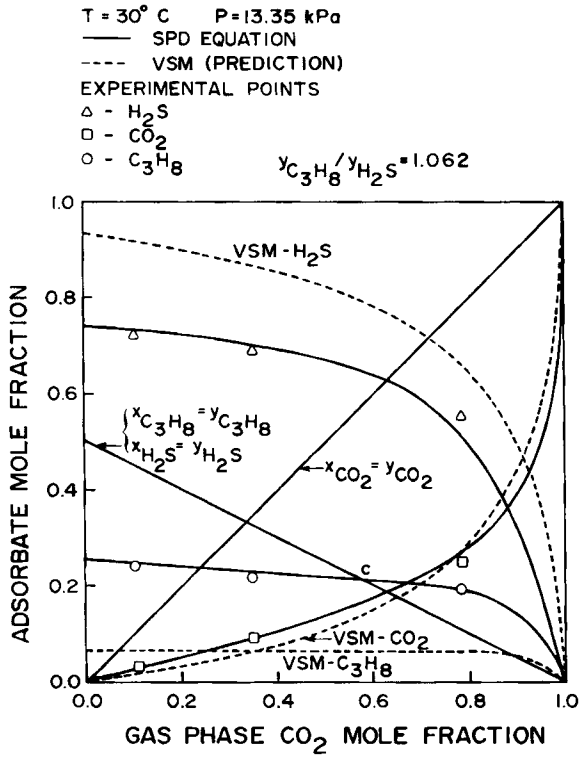

Figure 12. Ternary adsorbed phase compositions along CO_2 path (path *GH*).

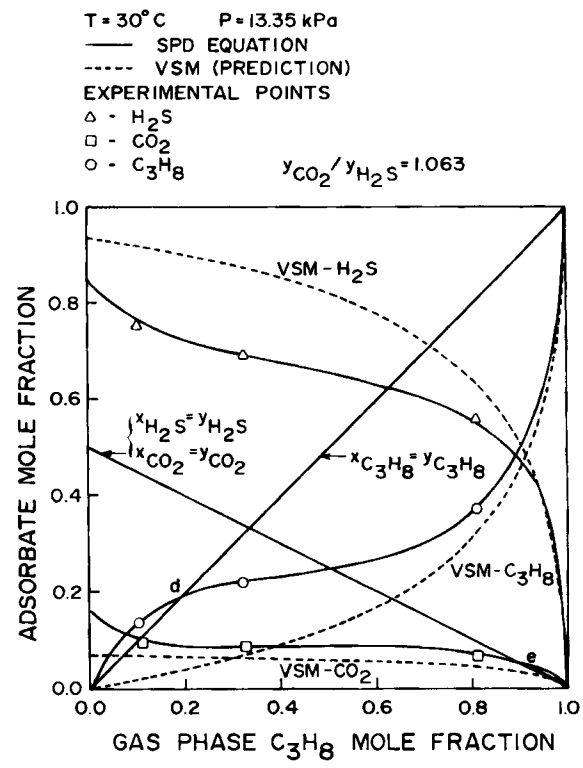

Figure 13. Ternary adsorbed phase compositions along C_3H_8 path (path *EF*).

Along the binary edges (*CE* and *GE*), the H_2S and CO_2 composition curves are mirror images of the C_3H_8 composition curves with crossovers; thus along segment *CL* of the H_2S—C_3H_8 binary $x_{H_2S} < y_{H_2S}$, while along segment *DE* of the CO_2—C_3H_8 binary $x_{CO_2} > y_{CO_2}$.

As CO_2 is added to the H_2S—C_3H_8 binary along segment *CL* the mixture moves into the ternary region labeled III, and the intensity of the H_2S—C_3H_8 competition is diminished. Eventually the propane composition becomes so low that the mixture assumes the character of the H_2S—CO_2 binary where the $x_{H_2S} > y_{H_2S}$. Thus an H_2S crossover must occur along $\overline{CbL}$, which divides regions I and III.

As H_2S is added to the CO_2—C_3H_8 binary along segment *DE*, the mixture moves into the ternary region labeled IV, and the intensity of the CO_2—C_3H_8 competition is overwhelmed by the more strongly adsorbed H_2S. Eventually, the CO_2 preference in the adsorbed phase is overshadowed by the H_2S preference so that a CO_2 composition crossover occurs along $\overline{EegD}$, which divides regions II and IV.

Ternary isotherm predictions

Along with the experimental results, calculated equilibrium data are shown in Figures 11, 12, 13. The vacancy solution model (VSM) predicts only one azeotropelike crossover, a C_3H_8 crossover along the CO_2 path. Even this point is displaced from the experimental data. In predicting the composition the VSM comes fairly close to the CO_2 curves along all three component paths; however, it overestimates the H_2S compositions while it underestimates the C_3H_8 compositions.

The spreading-pressure-dependent (SPD) equation predicts

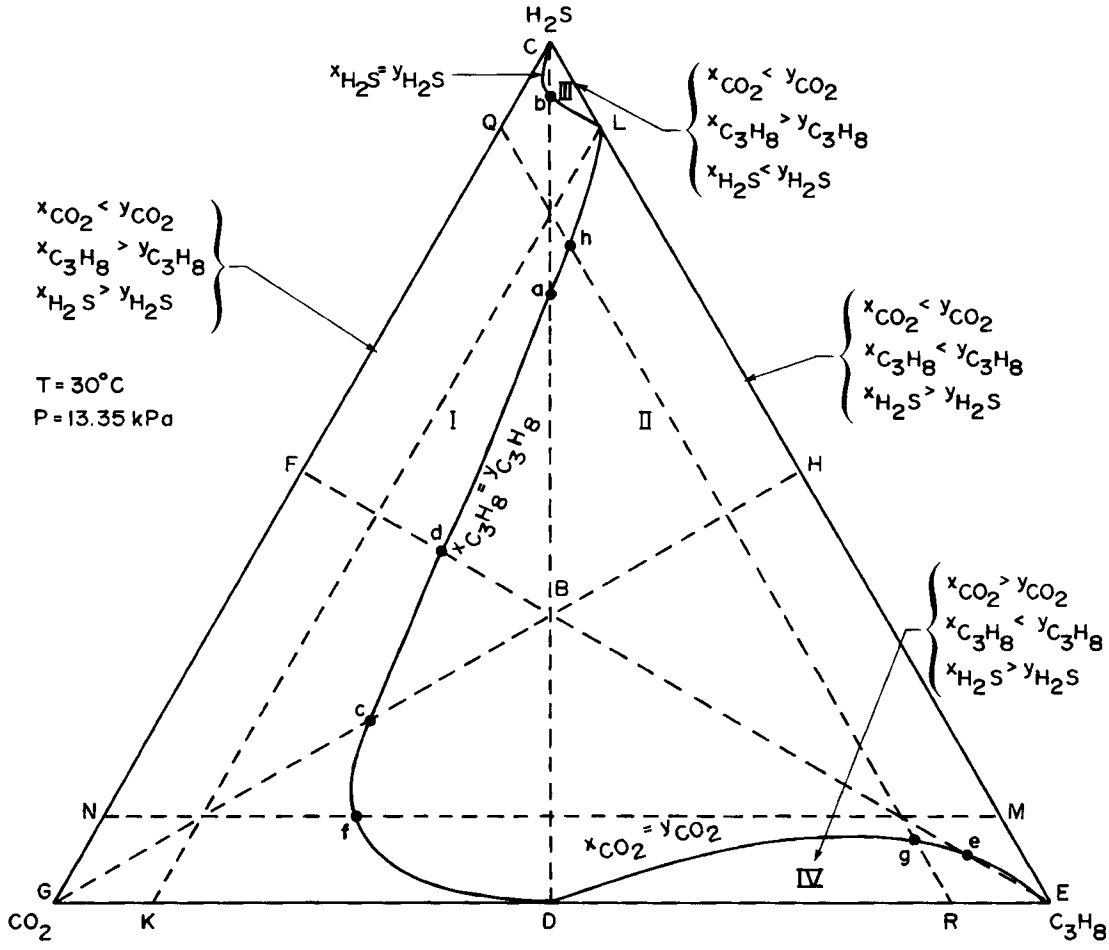

Figure 14. Triangular composition diagram at constant temperature and constant pressure.
Locus of composition crossovers for ternary mixture

the experimental data with good accuracy. Using the parameters obtained from the binary data, the SPD equation predicted the ternary data with a 5% accuracy, indicating the general applicability of the equation. The SPD equation is purely predictive for the ternary system studied.

To further demonstrate the importance of using the spreading-pressure dependence of the activity coefficients in the calculation of multicomponent adsorption equilibrium data, the values of the total amount adsorbed were calculated by applying Eq. 2. These results are tabulated in Table 7. The first summation term on the righthand side of Eq. 2 represents the ideal solution value of the total amount adsorbed. The difference between the ideal solution and actual values (i.e., the difference between columns *4* and *7* in Table 7) shows that significant errors can be encountered when the spreading-pressure dependence is neglected.

Using Eq. 2 in conjunction with the SPD equation, the total amount adsorbed vs. gas phase composition surface at constant temperature and constant total pressure was calculated, and these results are presented in orthogonal representation in Figure 15. As indicated above, the surface exhibits a maximum in the trisection near the H_2S vertex. The dashed curve in Figure 15 is the boundary of the peak region and it is labeled $n > n^{\circ}_{H_2S}$, since the single-component H_2S corresponds to the ideal solution maximum. The absolute peak can be located at the composition coordinates $y_{H_2S} = 0.91$, $y_{CO_2} = 0.02$, and $y_{C_3H_8} = 0.07$. Without the second summation term in Eq. 2, which accounts for the spreading-pressure dependence of the activity coefficients, which in turn represents the nonidealities of the system, the peak would not have been predicted. The ideal system surface would be situated between the single-component values of H_2S as the largest amount adsorbed, and of C_3H_8, as the least amount adsorbed. The experimental data, although not shown in Figure 15, were matched by the calculated values within 5% accuracy. It is noteworthy that using the activity coefficient correlations that do not include the spreading-pressure dependency, i.e., RAST model, does not predict the peak in the amount adsorbed surface.

Conclusions

The adsorption system of CO_2, H_2S, and C_3H_8 on H-mordenite exhibits nonidealities, as evidenced by the azeotropic behavior in the composition domain and by the peaks in total amount adsorbed. Consistent patterns of nonidealities were observed for the three binary systems and the ternary system, and they can be qualitatively explained by the molecular competition between the component species. These results are thermodynamically consistent and they have been used to test multicomponent adsorption models.

Table 7. Ternary Equilibrium Data of H_2S, CO_2 and C_3H_8 Mixtures on H-mordenite

Pressure kPa	Gas Phase Composition* y_{CO_2}	Gas Phase Composition* y_{H_2S}	Actual Total Amount Adsorbed n	Adsorbed Phase Composition* x_{CO_2}	Adsorbed Phase Composition* x_{H_2S}	Ideal Solution Total Amount Adsorbed n^i	Deviation from Ideality $\frac{n-n^i}{n}\times 100$
			Constant Gas Composition				
0.65	0.364	0.318	0.92	0.092	0.775	0.72	21.7
3.25	0.371	0.320	1.44	0.087	0.718	1.19	17.4
6.85	0.388	0.299	1.65	0.097	0.687	1.55	6.1
13.42	0.349	0.326	1.87	0.091	0.630	1.65	11.8
			Constant Gas Pressure; CO_2 Path; $y_{C_3H_8}/y_{H_2S} \approx 1.0621$				
13.36	0.108	0.431	1.95	0.031	0.729	1.71	12.3
13.42	0.349	0.326	1.87	0.091	0.690	1.65	11.8
13.34	0.785	0.101	1.65	0.251	0.553	1.40	15.2
			Constant Gas Pressure; H_2S Path; $y_{C_3H_8}/y_{CO_2} \approx 0.9635$				
13.33	0.443	0.098	1.72	0.161	0.532	1.31	23.8
13.42	0.349	0.326	1.87	0.091	0.690	1.65	11.8
13.33	0.097	0.814	1.99	0.022	0.868	1.93	3.0
			Constant Gas Pressure; C_3H_8 Path; $y_{CO_2}/y_{H_2S} \approx 1.0630$				
13.33	0.445	0.449	1.90	0.100	0.763	1.76	7.4
13.42	0.349	0.326	1.87	0.091	0.690	1.65	11.8
13.68	0.102	0.091	1.69	0.069	0.056	1.22	27.8

*$y_{C_3H_8}$ and $x_{C_3H_8}$ can be calculated since $\Sigma_{y_i} = 1$ and $\Sigma_{x_i} = 1$.

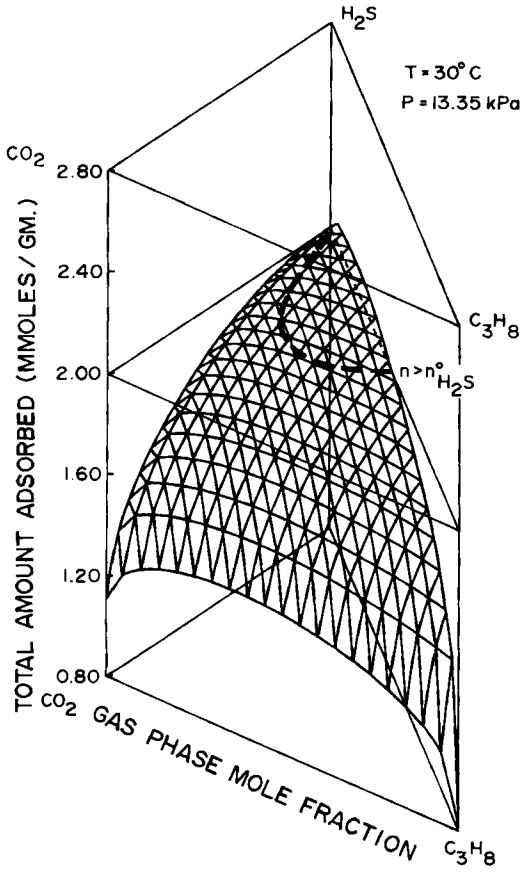

Figure 15. Orthogonal representation of total amount adsorbed at constant temperature and constant pressure for ternary mixture.

The SPD equation with parameters determined from single-component and binary adsorption data gives excellent prediction of the ternary equilibria. Also, the significance of spreading-pressure dependency of the activity coefficients was demonstrated. By neglecting this dependence a pseudoactivity coefficient is generated that will account for the nonidealities on a localized, point-by-point basis.

Notation

A = total area of adsorbent
a = molar area of adsorbate
a^m = molar area change upon mixing
a_i^o = single-component molar area at standard state (at same spreading pressure and temperature as the mixture)
C = number of components in adsorbate mixture
e_{ij} = average lateral interaction potential between segments of molecules i and j
M = Avogadro number
n = total amount adsorbed
n_i^o = single-component amount adsorbed at standard state (at same spreading pressure and temperature as mixture)
P = total gas phase pressure
P_i^o = standard state gas pressure during single-component adsorption (at same spreading pressure and temperature as mixture)
q_j^{st} = single component isosteric heat of adsorption of component j
R = gas constant
r = constant gas composition ratio for ternary experiments at constant pressure
s_j = shape factor of molecule j
T = absolute temperature
x_j = adsorbate phase composition of component j, mole fraction
y_j = gas phase composition of component j, mole fraction
z = coordination number for the array of segments

Greek letters

α_{ij} = Boltzman weighting factors for local segment compositions, Eq. 11

β_{ij} = cross-lateral interaction correction parameter
γ_i = adsorbate phase activity coefficient of component i
π = spreading pressure
ϕ_j = overall external contact fraction of j molecules in the mixture, Eq. 10

Superscripts

o = pure-component phase
i = ideal solution property
m = mixing property

Subscripts

i, j, k, m = component indices

Literature cited

Abrams, D. S., and J. M. Prausnitz, "Statistical Thermodynamics of Liquid Mixtures: A New Expression for the Excess Gibbs Energy of Partly or Completely Miscible Systems," *AIChE J.*, **21,** 116 (1975).

Barrer, R. M., "Specificity in Physical Sorption," *J. Colloid Int. Sci.*, **21,** 415 (1966).

Costa, E., J. L. Sotelo, G. Callega, and C. Marron, "Adsorption of Binary and Ternary Hydrocarbon Gas Mixtures on Activated Carbon, Experimental Determination and Theoretical Prediction of the Ternary Data," *AIChE J.*, **27,** 5 (1981).

Gugenheim, E. A., *Mixtures,* Clarendon Press, Oxford (1952).

Hyun, S. H., and R. P. Danner, "Equilibrium Adsorption of Ethane, Ethylene, Isobutane, Carbon Dioxide, and their Binary Mixtures on 13X Molecular Sieve," J. Chem. Eng. Data, **27,** 196 (1982).

Kingston, G. L., and A. L. MacLeod, "Heats of Sorption of Gases in Chabazite, Energetic Heterogenity and the Role of Quadrupoles in Sorption," *Trans. Faraday Soc.*, **55,** 1799 (1959).

Markham, E. C., and E. F. Benton, "The Adsorption of Gas Mixtures by Silica," *J. Am. Chem. Soc.*, **53,** 497 (1931).

Maurer, G., and J. M. Prausnitz, "On the Derivation and Extension of the UNIQUAC Equation," *Fluid Phase Equilibria,* **2,** 91 (1978).

Moore, W. J., *Physical Chemistry,* 3rd ed., Prentice-Hall, Englewood Cliffs, NJ (1962).

Myers, A. L., "Activity Coefficients of Mixtures Adsorbed on Heterogenous Surfaces," *AIChE J.*, **29,** 691 (1983).

Myers, A. L., and J. M. Prausnitz, "Thermodynamics of Mixed Gas Adsorption," *AIChE J.*, **11,** 121 (1965).

Perfetti, G. A., and J. P. Wightman, "Adsorption of Mixed Vapors on Solids. II: Cab-O-Sil," *J. Coll. Interface Sci,* **55,** 252 (1976).

Ross, S., and J. P. Oliver, *On Physical Adsorption,* Wiley, New York (1964).

Suwanayuen, S., and R. P. Danner, "Vacancy Solution Theory of Adsorption from Gas Mixtures," *AIChE J.*, **26,** 76 (1980); *AIChE J.*, **26,** 1968 (1980).

Talu, O., "Thermodynamics of Multicomponent Gas Adsorption Equilibria of Nonideal Mixtures," Ph.D. Diss. Arizona State Univ., Tempe (1984).

Manuscript received Mar. 5, 1985, and revision received Dec. 26, 1985.